Positron Emission Particle Tracking (PEPT) for the analysis of water motion in a domestic dishwasher

Pérez-mohedano, R.; Letzelter, N.; Amador, C.; Vanderroest, C.t.; Bakalis, S.

DOI:
10.1016/j.cej.2014.08.033

Document Version
Publisher's PDF, also known as Version of record

Citation for published version (Harvard):
Pérez-mohedano, R, Letzelter, N, Amador, C, Vanderroest, CT & Bakalis, S 2015, 'Positron Emission Particle Tracking (PEPT) for the analysis of water motion in a domestic dishwasher', *Chemical Engineering Journal*, vol. 259, pp. 724-736. https://doi.org/10.1016/j.cej.2014.08.033

Chemical Engineering Journal 259 (2015) 724–736

Contents lists available at ScienceDirect

Chemical Engineering Journal

journal homepage: www.elsevier.com/locate/cej

Positron Emission Particle Tracking (PEPT) for the analysis of water motion in a domestic dishwasher

R. Pérez-Mohedano [a,b,*], N. Letzelter [b], C. Amador [b], C.T. VanderRoest [c], S. Bakalis [a]

[a] Centre for Formulation Engineering, Department of Chemical Engineering, University of Birmingham, Edgbaston, Birmingham B15 2TT, UK
[b] Procter & Gamble Innovation Centers Ltd., Whitley Road, Longbenton, Newcastle Upon Tyne NE12 9TS, UK
[c] Whirlpool Corporation, Benton Harbor, Michigan, MI 49022, USA

HIGHLIGHTS

- We characterised water motion inside a domestic dishwasher via Positron Emission Particle Tracking (PEPT).
- Water distributes detergents and provides the mechanical force required to remove soils.
- Five stages identified: movement inside internal equipment and spray arm, ejection, impact, downfall and recirculation.
- Jet paths were observed to follow a straight line.
- Results have been used to validate Computational Fluid Dynamic (CFD) simulations.

ARTICLE INFO

Article history:
Received 29 January 2014
Received in revised form 6 August 2014
Accepted 13 August 2014
Available online 20 August 2014

Keywords:
Positron Emission Particle Tracking (PEPT)
Automatic dishwashing
Fluid mechanics
Computational Fluid Dynamics (CFD)
Radioactive tracer

ABSTRACT

Motion of water inside a household dishwasher has been characterised via Positron Emission Particle Tracking (PEPT). The technique enables the visualisation of the motion of a radioactive tracer in three-dimensional and opaque systems. Results showed a periodic sequence of the water over time, encompassing the following steps: movement inside internal equipment and spray arm, ejection via jets, impact over walls and crockery, downfall (either over walls, crockery or free falling) and recirculation of the bulk water from the bottom of the dishwasher. This sequence was shown to occur within a few seconds and the highest velocities, and therefore, the highest kinetic energies, were found upon ejection. Jet paths were observed to follow a straight line. Increased pump speeds increased velocity ejection profiles, but the effect over the downfall step was negligible. In fully loaded dishwasher (with crockery), the tracer moved slower in these high packing zones, showing low velocity profile areas with higher residence times. Other stagnant areas were found at the edges of the bulk of water remaining at the bottom of the dishwasher. Use of detergent did not seem to affect water motion. Finally, data generated via CFD was compared with equivalent PEPT data, showing good agreement for the spray arm and ejection steps but disagreement in the free falling step. The divergences in the results can be explained by a combination of PEPT data processing and CFD model constraints. Information gathered is helping the development of more sustainable and efficient dishwashing systems.

1. Introduction

Electrical household appliances, such as Automatic Dishwashers (ADW), have eased housework tasks. According to a recent study [1] of consumers in the UK, automatic dishwashing shows important benefits on time saving and water consumption. The typical time needed to load and unload the dishes is around 9–10 min, whilst hand washing the same standardised load [2] could take up to 60 min. The amount of water used by hand washing is around 49 L on average and this amount is reduced to 13 L with a dishwasher. In terms of energy consumption (mostly used for heating water), this study shows a use of 1.7 kWh on average for hand washing and 1.3 kWh for automatic dishwashing. A higher use of this type of household appliances would lead to environmental benefits as a significant proportion of energy and water consumption worldwide occurs in the domestic sector.

* Corresponding author at: Centre for Formulation Engineering, Department of Chemical Engineering, University of Birmingham, Edgbaston, Birmingham B15 2TT, UK. Tel.: +44 74 111 69186.
E-mail addresses: PMR005@bham.ac.uk, rpmohedano@gmail.com (R. Pérez-Mohedano).

http://dx.doi.org/10.1016/j.cej.2014.08.033
1385-8947/

Despite its common use, cleaning processes occurring inside Automatic Dishwashers (ADW) are not simple nor well understood. Scientific information related to dishwashers is scarce and mostly associated to energy consumption and water savings. A heat recovery design from wastewater was studied by De Paepe et al. [3] to heat fresh water and enhance energy efficiency. Weiss et al. [4] analysed the additional potential in energy efficiency that exists for household appliances, including dishwashers. A different approach was followed by Asteasu et al. [5] to demonstrate CAD capabilities on analysing flow pattern problems and geometrical design. Water jets patterns over a plate were used as a proof of concept. However, a detailed study of the characteristics of an ADW is necessary to build the in-depth knowledge and fully understand the wash process.

Dishwashers are complex systems in which a combination of chemistry, temperature, water flow and inner properties of soils are evolving dynamically during a wash cycle. Four areas can be identified: (1)dishwasher design and operation parameters, (2)dishwasher load and type, (3)types of food soils and (4)detergent formulation. The key element that links all areas together is water. It is responsible for the variation in the total cleaning time. Water produces shear stresses over crockery items by direct impact of the water jets, transports the chemistry onto the soils, dissolves certain types of foodstuff and removes low adhesive soils after penetration of chemistry. Therefore, among different parameters, water distribution plays a very important role when analysing the performance of the system.

1.1. Cleaning mechanisms and soil properties

Complex soils mixtures can be found typically in an ADW. Fryer and Asteriadou [6] proposed a classification for cleaning phenomena based on types of soils and mechanisms of removal. Soils were classified based on their physical properties, ranging from *low viscosity fluids* to *cohesive solids*. Cleaning fluids were classified from *water at ambient* to *hot chemicals*.

For cleaning to occur, cohesive forces that bind the soil together and adhesive forces that bind the soil with the substrate must be overcome. If no chemicals are needed and fluid flow is enough, the mechanism can be known as *fluid mechanic removal*. If chemical presence is necessary, a *diffusion–reaction removal* will happen. A combination of different dynamics processes can occur at the same time. These involve mass transfer between the soil-fluid, diffusion of actives species into the soil and reactions of some chemicals that change the inner physical properties. The soil structure is firstly weakened and cleaning eased at the end. Depending on the rate limiting stage, the removal path will occur in a different way.

1.2. Impinging jets

Rotating jet spray arms are used to distribute water in ADW. The coverage produced on the surface by the water jets and the shear stress thus generated are believed to be key factors for the effectiveness of cleaning [7]. The impact of an impinging jet over a flat surface makes the liquid move outward radially in a thin film at high velocity. After some distance 'R' (see Fig. 1), the fluid forms a thicker film as it reaches the film jump. The film jump is defined as the point where a liquid moving fast gets onto a small velocity profile area, producing a sudden decrease in its velocity and thus, an abrupt increase in the liquid height. Then, the liquid drains downwards and forms a falling film of width '*W*'. The term *film jump* is differentiated from the traditional *hydraulic jump* as the latter typically refers to the transition region over horizontal surfaces, where gravity does not affect the fluid flow [8].

Net contributions from gravity, surface effects and the inclination of the impingements coherent jets create a range of down flow behaviours [9,10]. Three common types are known as 'Gravity flow', 'Rivulet flow' and 'Dry Patch' (see Fig. 1). The latter two cases are undesirable for cleaning purposes:

- *Gravity flow:* The liquid drains as a thin film with a width 'W_G'. This width is related to the maximum liquid radius at the impingement proximities. Gravity contributions dominate over surface effects.
- *Rivulet flow:* The liquid film shrinks and forms one or more tails of width 'W_R'. Surface tension effects are in the range of gravity contributions.
- *Dry Patch:* The falling film splits into two. Again surface tension effects are equally important than gravity contributions.

Within an ADW, impinging jets may impact the different surfaces at a wide range of angles. Overall, the same principles are applied. Also, other water distribution patterns are produced: splashing of water due to a jet breaking or falling film generated due to the accumulation of water from top positions. These aspects are hardly quantifiable, and therefore the scope of this work will be focus only on jets movement and characterisation.

Different angles of ejection are obtained by varying the design of the individual nozzles present in a spray arm and by changing the pump pressure. This produces different ejections paths depending on the nozzle considered. Also, the spray arm rotation rate is a consequence of a total torque generated. Generally, the presence of one or more 'driving nozzles' at the bottom of a spray arm creates a net force due to the reaction force (third Newton's law) that is produced on the spray arm once the water is ejected.

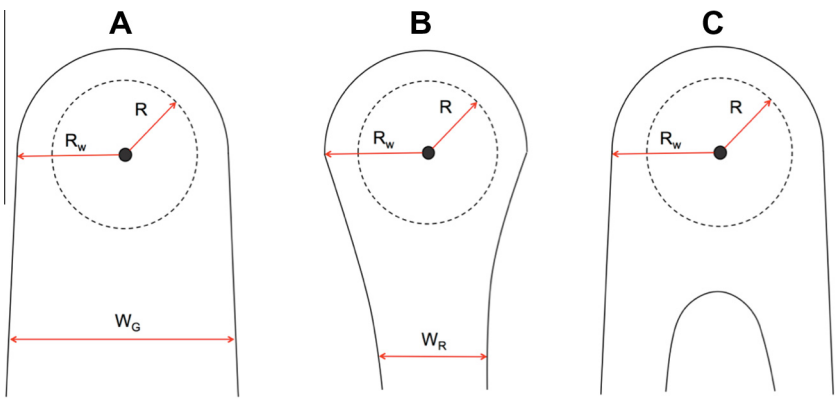

Fig. 1. Drainage flow patters after impingement of a jet over a vertical surface. Black dot represents impingement point. (A) Gravity flow. (B) Rivulet flow. (C) Dry patch. Legend: R = film jump radius; R_W = external circumferential radius; W_G = gravity flow film width; W_R = rivulet flow film width.

1.3. Positron Emission Particle Tracking (PEPT)

For the analysis of water motion, the University of Birmingham developed a technique called Positron Emission Particle Tracking (PEPT), which enables non-invasive 3D spatial detection of a radioactively labelled particle (tracer). One of the greatest advantages of this technique is that can be used for the analysis of flow within opaque systems containing metals [11].

Throughout the years, the technique has been used successfully in a wide range of experimental set-ups. Barigou [12] gave a good overview of the capabilities of PEPT. Bakalis et al. [13] were able to measure velocity distributions of different viscous fluids within a pipe. As an example, a field widely studied has been mixing systems [14]. Extensive research hasbeen done in rotating systems [15], such as in tumbling mills [16], or for studying the segregation of different sized particles [17]. Additionally, PEPT has been recently used to characterise the motion of textiles in a front-loading washing machine [18] showing its capability to characterise flow in household appliances.

Comparisons between PEPT experiments and CFD simulations have also been done. Studies on the suspension distribution of monodisperse particles in water were performed by using both techniques [19,20]. Results showed good agreement between CFD and PEPT data. Some discrepancies were found in areas with important velocity or directional particle changes. PEPT technique has been also compared to other commonly used visual techniques, such as Particle Image Velocimetry (PIV) [21]. Benefits of PEPT for the analysis of opaque systems were proved and good agreement was again found between both techniques.

In this work, Positron Emission Particle Tracking is used for the analysis of water flow in a typical dishwasher. Characterising water flow in ADWs is critical to create the foundational work required to link physical and chemical phenomena since water is the key element driving both. A typical water sequence was determined and Lagrangian velocities estimated. Eulerian flow-field studies are performed to determine velocity profiles and residence time distributions over the inner volume of the ADW. Finally, PEPT data is compared with CFD data using the same experimental conditions.

The system shows the peculiarity of not being completely filled with water as jets are sprayed within the inner volume. Therefore, this study can also be used as a proof of concept for similar systems (i.e. sprinklers or pipe cleaning sprayballs).

2. Materials & methods

2.1. Dishwasher set-up

Experiments were carried out in a customised Whirlpool (DU750) dishwasher with internal loading area dimensions of 560 × 500 × 620 mm (Width × Depth × Height). Crockery was distributed in two baskets situated at different heights and three spray arms with different designs distributed the water all around the dishwasher. The software controlling the different washing cycles was modified to offer different water pump speeds and the selection of the spray arm ejecting water. Washing time of the customised cycles could be up to 3 h. Fig. 2 illustrates the ADW set-up between the two PEPT cameras, the distribution of crockery and the coordinate system used as a reference. The origin of it was located at the middle bottom side of the ADW, in line with the axis of rotation of the spray arms.

Table 1
Experimental variables considered.

Variable	Condition
Pump speed	High Medium Low
Presence of load	'No baskets and No load' 'With baskets and load'
Detergent use	'No detergent' 'With detergent'

Commercially available crockery used was a combination of 12 dinner plates (D = 270 mm), 24 dessert plates (D = 160 mm), 12 teacups (D = 70 mm; H = 60 mm), 12 glasses (D = 65 mm; H = 120 mm) and 12 bowls (D = 120 mm). These items are used in standardised AHAM (Association of Home Appliance Manufacturers) industry tests. Loading of the dishwasher took place according to the method: dinner plates and dessert plates were placed in the lower basket and small crockery items in the upper basket [22]. 5 L of water were added at the beginning of each test with a temperature varying between 18 and 20 °C. The water-heating element was disabled, as the purpose of the experiments was not to analyse the effect of temperature. Variations in water density and viscosity, which could affect the flow, are negligible in the range of temperatures used. They were measured and remained constant through the cycles. A typical concentration of 3.4 g/L of powder detergent was used to identify the effect of cleaning formulation with flow. The lower spray arm was selected to be the only one spraying water.

Table 1 shows different conditions available to be analysed. Combinations of them were studied during the realisation of these tests.

2.2. PEPT set-up

For every experimental condition, radioactive tracers having diameters between 250 and 400 μm were used. Tracers were made using the resin ion-exchange procedure explained by Parker & Fan [23]. They were coated with blue paint to enhance their visibility

Fig. 2. (A) Dishwasher in between PEPT cameras. (B) Dishwasher loaded with crockery and cartesian coordinates reference system.

Table 2
Stokes values.

	High pump speed	Medium pump speed	Low pump speed
Spray arm	1.1	0.88	0.63
Ejection	39.1	26.1	13.0
Down flow over walls/ plates	10.3	10.3	10.3

and to prevent the spread of activity in the aqueous environment. A single tracer was introduced at the beginning of every experiment in the bulk of water that remains at the bottom of the dishwasher. Data was collected for 30 min on average. The radioisotope used (^{18}F) has a half-life of 109 min. However, tracers still presented an acceptable radioactivity 4 h after their production.

The ability of the tracer to follow the fluid flow is characterised by the Stokes number ($St = \tau_p/\tau_f$), where τ_p ($\tau_p = \rho_s d_p^2/18\mu_f$) is the particle response time and τ_f ($\tau_f = d_c/U_o$) is the fluid response time to an external disturbance. For $St < 1$, the particle is considered to follow closely the fluid streamlines while if $St > 1$, particle's inertia forces will start to influence particle's movement [24].

For these calculations, the worst cases were considered for every experimental setup: highest particle diameter ($d_p = 400$ μm) and highest velocities found (U_o). Tracers densities (ρ_s) were ~1100 kg/m^3 and water viscosity (μ_f) was ~0.001 Pa s. To calculate the characteristic dimension of the spray arm, a rectangular duct was assumed ($d_c = 2LW/(L + W)$) with $L = 0.01$ m and $W = 0.035$ m. The characteristic dimension in the ejection step was assumed to be the most common nozzle diameter (0.002 m) in the design of the lower spray arm. For the down flow over the walls or plates, the characteristic dimension was interpreted as the thickness given when a homogeneous distribution of the amount of ejected fluid (not at the bottom or in the internal pipes) is covering all those surfaces (estimated thickness = 0.0009 m). Table 2 summarises maximum Stokes numbers calculated for every condition.

Results show low values for the spray arm flow, which agrees with the isokinetic assumption. For the ejection part and downfall stages, higher values than 1 are found. A deviation of the particle's behaviour from the fluid flow is therefore expected. The higher density from the tracer might make the particle to show higher resistance in the ejection path and to travel within the lowest layers (slower) of the fluid film during the downfall. However, the ejection step is very rapid in time, as it will be seen in Section 3.1, and the deviation due to the inertia forces of the particle are assumed negligible.

The field of view of PEPT cameras is about 300 × 600 mm (Depth × Height). Taking into account that at the edges the quality of the data can be highly compromised [11], only the flow between the lower and medium spray arm was analysed.

2.3. Data analysis

2.3.1. Pre-processing

Raw data obtained with PEPT consists of two dimensional locations corresponding to the position of gamma-ray detections in each of the cameras. A previously developed algorithm [11] was used to transform this initial raw data into three dimensional tracer locations.

Another algorithm was then developed to process the obtained positions. The steps taken were as follows:

I. An initial step removed all data with a spatial ***location error*** higher than 3 mm. Remaining data was hereinafter filtered out if its spatial location error was higher than the average spatial error value plus two times the standard deviation of the data not filtered initially.

II. Data was further ***smoothed*** following the procedure below:
   a. Initially, moving average intervals of **5**–**25** points were created with respect a central point (P_0).
   b. These intervals were then fitted using **1st**, **2nd** and **3rd** order polynomial equations (based on least squares method) and a new central point obtained (P_{new}).
   c. Then, for every specific combination of intervals sizes and fitting orders a matrix was created with new central points (P_{new}) for each original location. Distances between consecutive points were calculated and associated to every combination. The one that showed the smallest standard deviation was the combination selected at the end of the process and its new central points replaced the original data.
   d. As a restriction criterion, data was only smoothed if the 3D spatial distance within the moving average interval was less than **30** mm and/or if time difference for consecutive points was less than **0.1** s.

Fig. 3 shows an example of the smoothing process for a small amount of data. It can be seen how a new central point (black dot) is created for the case of an interval of 9 points (blue-green dots) and the use of a 2nd order polynomial equation (green dash-line). The new central points (red dots) for that combination are shown as well. Data not modified due to the application of the restriction criteria can be also seen (coincidence of blue and red dots).

III. It was expected to get fast moving tracers at the water jets. Due to the constant data acquisition time of PEPT cameras, the number of data points was lower at that stage. To solve a similar problem (systems with a wide range of velocities), Chiti et al. [25] applied a ***selective linear interpolation*** method. The authors achieved a more homogeneous spatial distribution of data points and increased the quality of the results. With that in mind, the application of this interpolation algorithm was used for spatial distances of consecutive locations between 5 and 20 mm. These values were chosen to be half and double the cell size (10 mm) for further Eulerian analysis. If spatial distances were smaller than the low

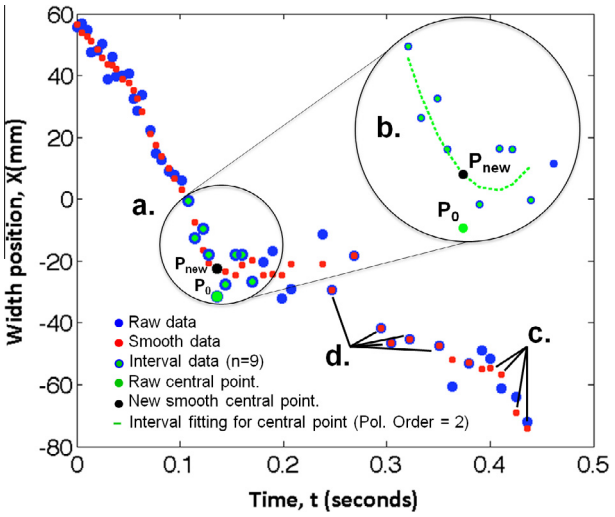

Fig. 3. Smooth data example. Blue dots – original Raw data; red dots – new smoothed data; blue-green dots – interval example ($n = 9$); green dot – interval central point (P_0); black dot – new central point (P_{new}); dotted green line – second order polynomial fitting for interval considered. (For interpretation of the references to colour in this figure legend, the reader is referred to the web version of this article.)

limit, no need for generating new points was required as data spatial distribution was good enough. When instead, spatial distances were bigger than the high limit, important errors could be introduced as a linear trajectory was considered for the interpolation.

2.3.2. Lagrangian velocities

Lagrangian velocities were estimated according to Mac Namara et al. [18]. A 'best fit' second order polynomial line was generated for every data point as a function of time. Then, the gradient of it was used as the Lagrangian velocity of the tracer. These values were optimised by taking different intervals of size '*n*', where '*n*' is the number of points used, and minimising the least squares error in the velocity calculation.

Depending on the situation, '*n*' value can be high or low. If the tracer were moving in a straight line, a high value of '*n*' would give a more accurate velocity. Whereas, if there was a sudden change in the trajectory, as for example in the spray arm ejection area (nozzles), less points would be required to follow accurately this change. Illustrations can be found in the paper cited above.

2.3.3. Eulerian analysis

Eulerian velocity data was represented graphically in a user-defined 2D cell grid, which divided the loading area into cells of equal size (10 mm). Lagrangian velocities were time-weighted averaged throughout each cell providing time independent Eulerian velocity values.

Considering the rotation of the spray arm, data was represented using a cylindrical coordinate system. Angular projection was disregarded, as the ejection pattern is not modified at different angular positions. This allowed a simpler way to look at the data and a 2D grid representation of it as a function of the tracer distance from the rotation axe (middle of the spray arm) and its height. Fig. 4 illustrates this transformation process.

Residence time plots represent the average time the tracer stays in every cell. These values were calculated as the tracer cumulative residence time divided by the number of passes.

2.4. Computational Fluid Dynamics

Computational Fluid Dynamics (CFD) data was generated by appliance manufacturer. For this study an unsteady state Eulerian multiphase model with VOF (volume of fluid) was considered. A Dynamic Fluid Body Interaction (DFBI) module was used to simulate the motion of the spray arm in response to the pressure and shear forces that the fluid exerted. The rotational motion around the vertical axis was made free, while motion over other axes was constrained. The moment of inertia was defined for the spray arm and the values were calculated in Pro-E software. The mass flow condition was applied at the inlet of the spray arm. A volume mesh was generated with polyhedral and prism layers, giving a total number of elements of 5 million. The time step size was kept constant at 10^{-4} s. The simulation was run in star-CCM+ with parallel processing on a cluster with 96 processors for 48 h. Post-processing was also done in star-CCM+.

The current simulation was carried out only for the lower spray arm with an empty (no dish-load, racks & silverware basket) dishwasher. Firstly, the flow field was developed through VOF multiphase simulation for two rotations of the spray arm. Then, a Lagrangian multiphase particle tracking was performed by using water particles (with all their physical properties considered). Particle diameters were decided based on water flow rate. Particles were sent through the inlet of the spray arm and tracked through each nozzle. The same coordinates system was created in Star-CCM+ as for PEPT experimental setup. Cartesian coordinates (*x*, *y* & *z*) of path traced as well as the velocity component associated to every location were recorded for each particle. A total number of 106 particles were sent through the inlet of the spray arm. A comparison between PEPT and CFD data is done in Section 3.4.

3. Results & discussion

Lagrangian and Eulerian velocities represented in this study have been non-dimensionalised with respect to the maximum velocity observed among all the experiments done. They represent the net vector velocity value.

3.1. Motion of the tracer particle

Fig. 5 shows a typical tracer path. The rapid increase in 'z' direction indicates an ejection from the lower spray arm and the decrease the downfall. The tracer was ejected every few seconds and appeared to follow a straight line (see further Section 3.2). Sometimes, parts of the particle paths were missing (i.e. time = 25 s), as particle locations could not be accurately detected. Above 0.6 Z_{max}, the tracer was outside the field of view of PEPT cameras and locations were not collected either. Most of the time the tracer was located at negative 'z' values, which corresponds to the bulk of water remaining at the bottom of the dishwasher.

Fig. 6 describes different steps of a typical ejection. Regardless of the presence of load (crockery and cutlery), the same pattern was observed: namely [(1)]movement inside the pump and spray arm, [(2)]ejection, [(3)]impact on the wall or crockery, [(4)]downfall (either over crockery, walls or free falling) and [(5)]back to the bulk

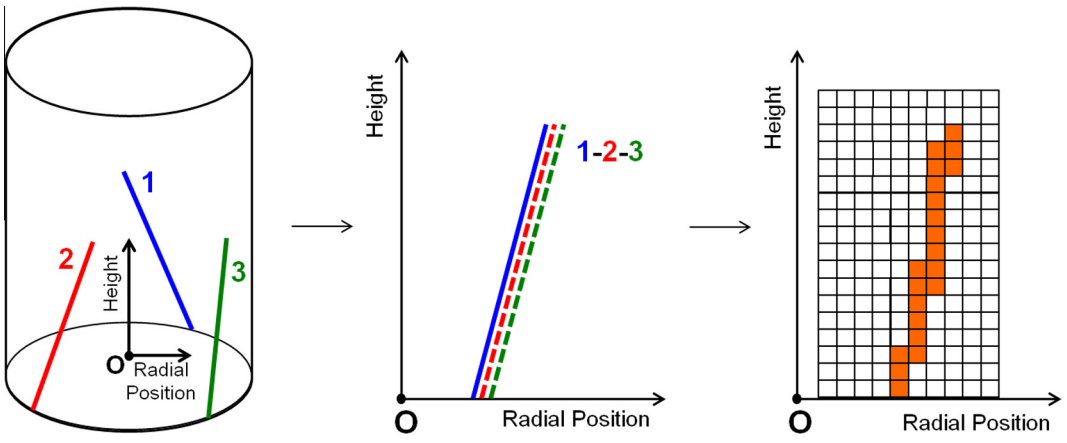

Fig. 4. Schematic of ejection patterns.

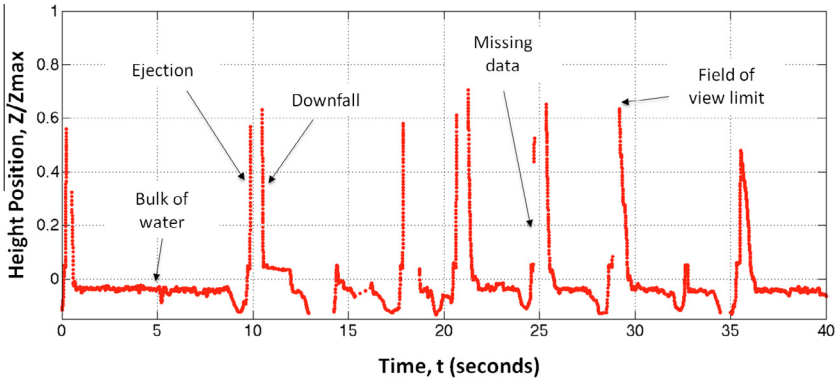

Fig. 5. Time series of a typical tracer path during an interval of 40 s in a wash cycle.

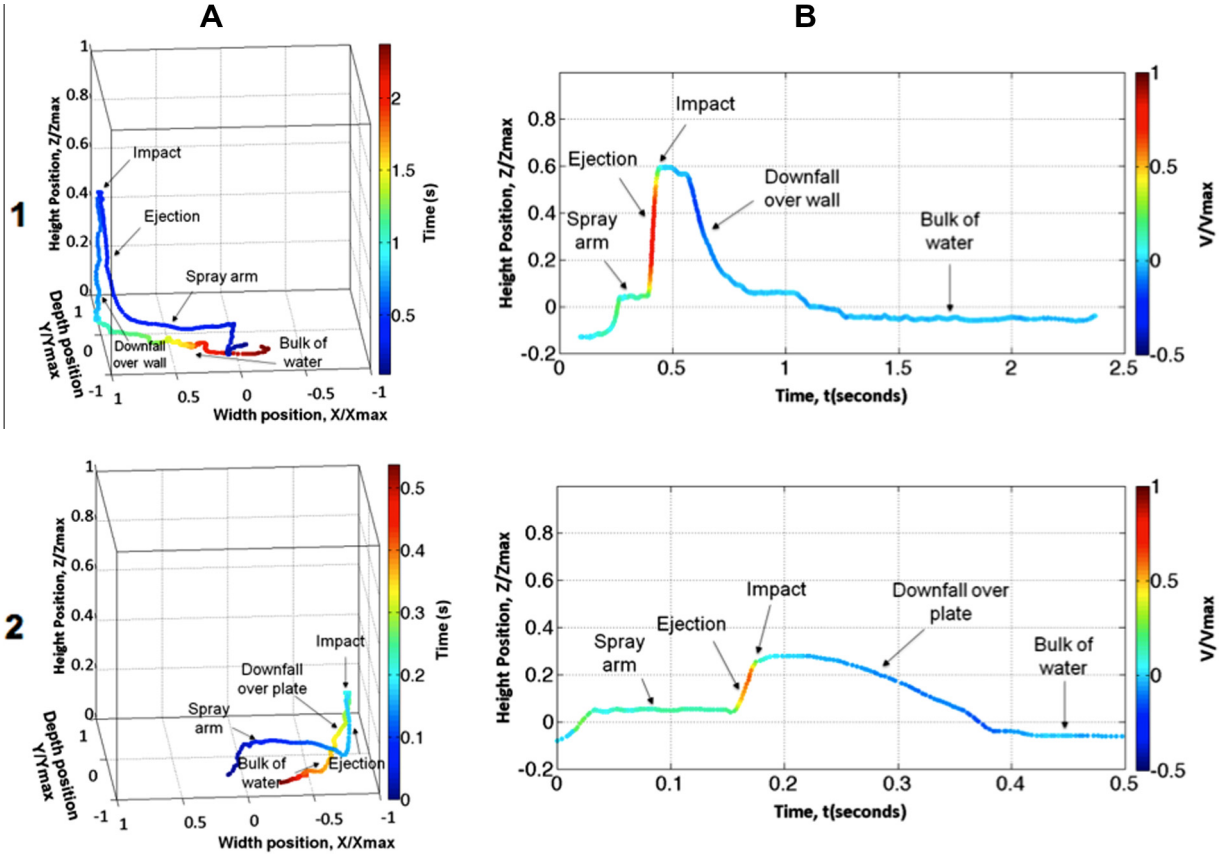

Fig. 6. Typical water sequence inside an ADW. 1 – 'No load'; 2 – 'With load'; (A) 3D plot scattered over time; (B) time sequence scattered over velocity.

of water. The time scale of the process was typically less than 3 s and the highest velocity values were found upon ejection.

The 'downfall over plate' stage (see Fig. 6B.2) happened within tenths of a second. The residence time is of importance in terms of the mechanism of transfer of surfactant/enzymes over the soils. As the amount of water present is not constant, cleaning phenomena are likely to differ from situations where soils are submerged constantly in cleaning solutions.

3.2. Characterisation of jets

Particle paths shown in Fig. 7 illustrate that once water was ejected the tracer moved in a straight line, with no effect on its trajectory from the rotation of the spray arm. This suggests that the rotational inertia given can be disregarded with respect to the vertical and radial components (considering a cylindrical coordinates system). Therefore, specific locations were targeted from specific ejection points. For a given time, jets trajectories can be considered as fixed vectors. A complete and constant coverage of areas with direct impingement of jets was also impossible due to this fact. Jets impact a specific location with a frequency related to the rotation rate of the spray arm.

Fig. 8 shows the fitting of a line in 3D space over multiple particle locations corresponding to an ejection. The analysis was done before the 'smoothing' and 'interpolation' steps (see Section 2.3.1), so any artificial change in the data that can cause interactions in the linearity was avoided. Linear fitting was done by estimating the line with the lowest error of approximation. This error was calculated as the sum of all orthogonal distances from the different tracer locations to the line (represented in Fig. 8A by the red lines)

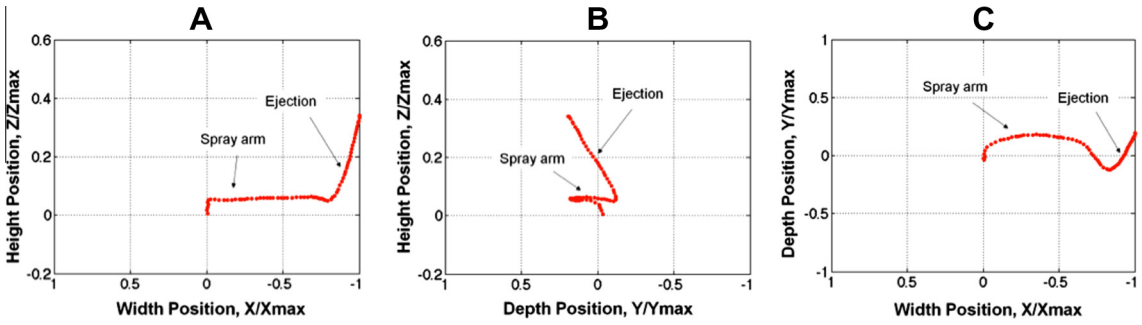

Fig. 7. Typical water jet path. (A) Front view. (B) Side view. (C) Upper view.

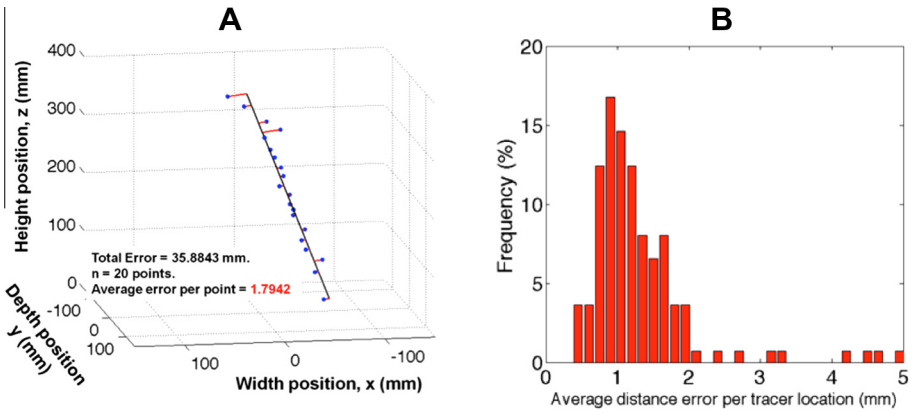

Fig. 8. (A) 3D fitting of tracer locations in an ejection stage. (B) Histogram of *R*-square values for the fitting of all ejection paths obtained. (For interpretation of the references to colour in this figure legend, the reader is referred to the web version of this article.)

and dividing this value by the number of locations considered. Therefore, an average distance error per tracer location was estimated for a single ejection analysed. Fig. 8B shows a distribution of the averaged distance error calculated for all the ejections seen. Most of the error values were found to be lower than 2 mm, with the highest concentration seen at values around 1 mm. These error distances fell within the inner tracer error per location as commented in Section 2.3.1. The low error values obtained agree with assumption of linearity in the water path once it is ejected.

In Fig. 9, a photo obtained through a high-speed camera shows the path that a single jet follows inside an ADW. Photos were taken through a Perspex® window replacing one of the sides of a commercially available dishwasher. The linearity in the jet trajectory was again observed.

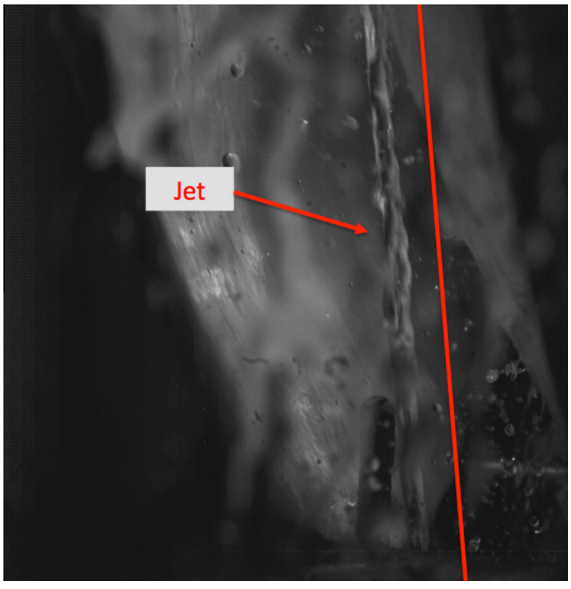

Fig. 9. High-speed camera capture from the inside of an ADW.

3.3. Eulerian analysis

As spray arms in ADW rotate around a fixed axis, cylindrical coordinates were used in the following analysis. A symmetry problem is spotted as loading of crockery occurs along a rectangular symmetry while the distribution of water is produced in a cylindrical-rotational way.

3.3.1. Velocity profiles

Fig. 10 illustrates velocity contours for different experimental conditions. Data was grouped as a function of the different steps of the sequential process explained in Section 3.1. As for a fixed cell location, up-flow and down-flow movement might co-exist, plots were divided in two rows to avoid any distortion in data analysis. Contours from tracer locations corresponding to the motion in the spray arm, injection and upward movement are shown in the first row. Contours from tracer down-flow movement and stay in the bulk of the water at the bottom are shown in the second row. Velocity values are given in absolute terms for an easier comparison. In the first row, tracer movement was ascending (ejection step) and followed the positive direction of the height axe. In the second row, the tracer movement was the opposite and followed the negative direction of the height axis. Velocity colour map scale

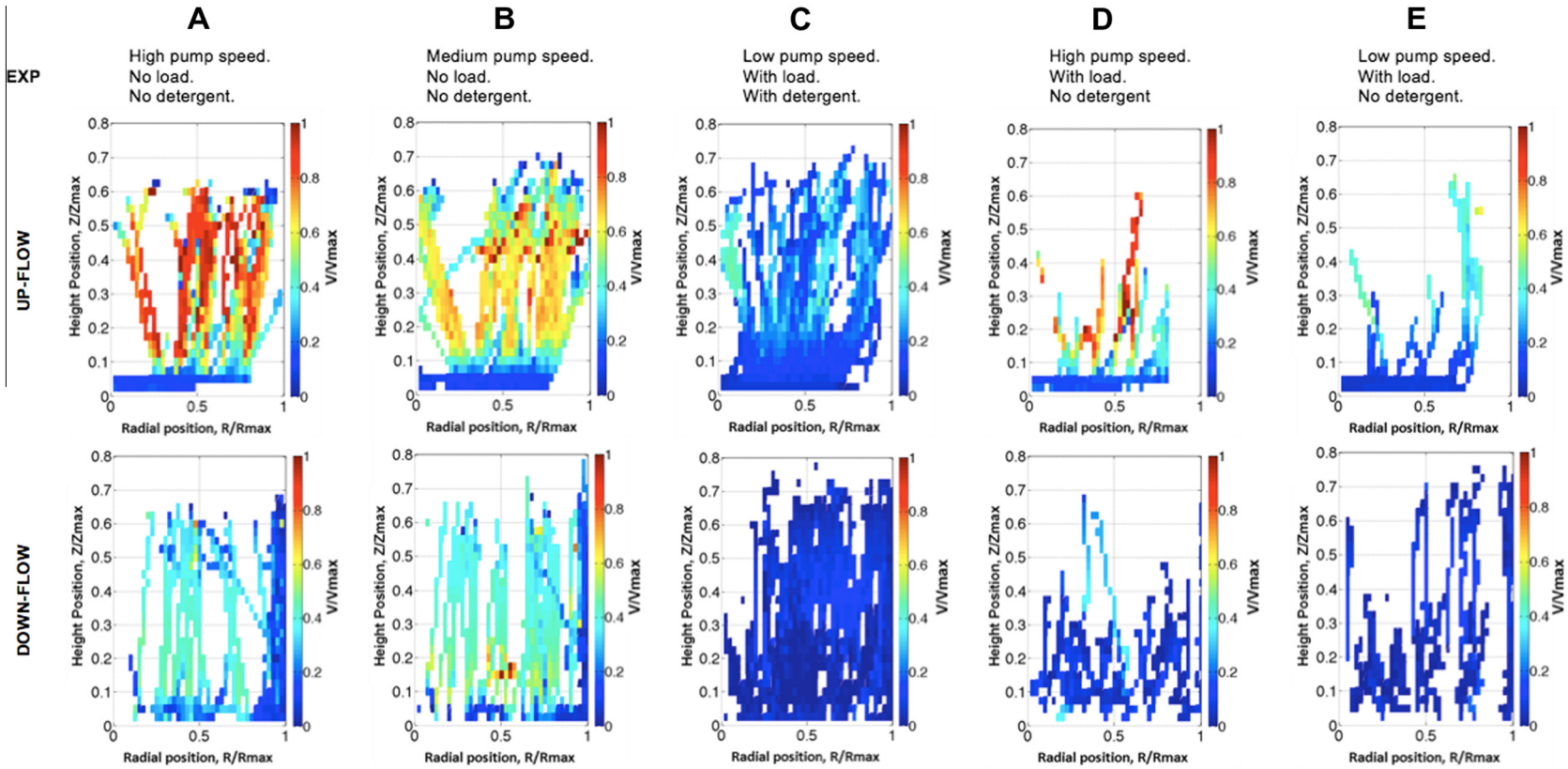

Fig. 10. Eulerian velocity distributions plots for 5 different experimental set-ups. Impact effect in up-flow movement has not being considered.

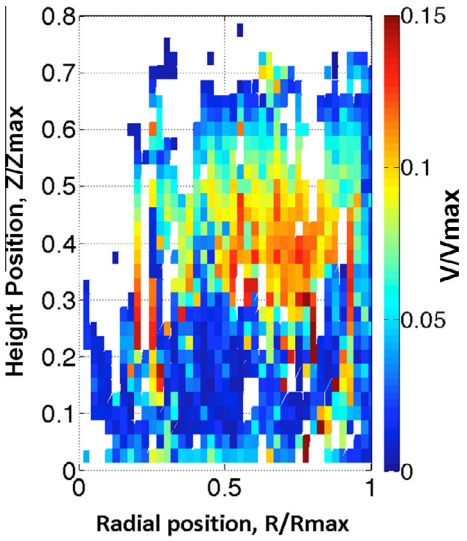

Fig. 11. Eulerian velocity plot for downfall stage. Experimental conditions: High pump speed, with load & with detergent.

was set to be the same for all plots shown, being the upper limit the highest velocity found over all experimental conditions.

In the first row, spray arm area is shown at heights below 0.05 Z_{max}. Above this height, velocity contours represent the tracer ejection movement. The impact of a water jet on surfaces was hard to characterise through these experiments, as the number of points collected for this phenomenon was quite small. For those experiments with 'no load', impact areas were found in dishwasher walls, that is, at high radial distances. However, with presence of load, impacts could happen anywhere, producing high distortions on data results (combination of high velocity values for ejections and low velocity values for impact). As a consequence, impact data was removed to preserve quality in the analysis. A small gap in coverage at around 0.35 R_{max} (radial position) was observed in Fig. 10A & B (first row). The specific design of the spray arm was responsible of this. The consequence was that water arriving at those areas did not come directly from a jet but from water being splashed or during the subsequent downfall step.

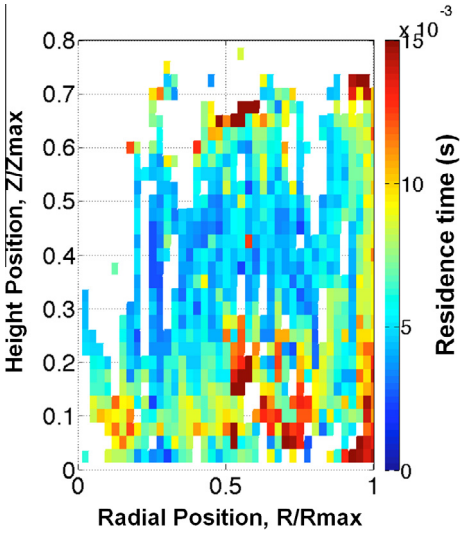

Fig. 12. Residence time contour for down-flow movement. Experimental set-up: Low pump speed, with load & with detergent.

Pump speed effect over the ejection velocity can be seen in Fig. 10A, B & C (first row). Tracers velocities increased for higher pump speeds as expected. Contours can be considered homogeneous over the whole ejection area (above 0.05 Z_{max}) and are not a function of the radial distance. A velocity transition was observed at the vicinity of the ejection points (heights between 0.05 Z_{max} and 0.1 Z_{max}). This effect will be analysed further in detail in Section 3.4.

In the second row, water downfall over the wall was found at high radial distances. From the Stokes number analysis, the tracer particle could be considered in this stage as a small soil substance and conclusions still be made. Low velocity values, corresponding to a dark blue colour, were seen. At lower radial values, two behaviours can be identified depending on the presence of load or not. In Fig. 10A & B (second row), and for cases where crockery was not present, tracer downfall inevitably followed a free falling movement driven by gravity from the roof of the dishwasher (pale blue to green colour). The same pattern was obtained independently of the *pump speed*, suggesting that the effect of the pump energy input is negligible over the downfall stages.

When *crockery was present*, tracer downfall velocities were reduced significantly, matching those velocities found at the walls for 'no load' conditions. Therefore, a system 'with load' can be seen as a succession of small walls grouped together. In Fig. 11, the velocity colour map scale was adapted for a typical experiment 'with load'. The upper limit in the scale was re-set to the highest velocity found in that contour plot to allow for a better distinction between areas in the downfall step. The lowest velocity values were found at a low height, corresponding to the bottom of the plates situated in the lower basket. Low velocity values were also found at the edge of PEPT cameras (~0.6 Z_{max}), where the top basket was located. From top positions, the tracer fell down and increased its velocity (from 0.6 Z_{max} to 0.3 Z_{max}). As it went down the likelihood to impact a plate increased. Once the impact happened, a reduction in velocity occurred (0.05 Z_{max}–0.3 Z_{max}). A sharp transition in velocity can be seen at heights around 0.3 Z_{max}. In this lower area, the tracer downfall velocity does not seem to change significantly. The high homogeneity found suggests that the distribution of shear stresses (mechanical energy input) over the crockery was low. Tracers were washed down at a very low speed even though they were gravity-aided. High velocity profile areas occurring before the film jump might had been very localised and spaced in time, thus they did not influence averaged results. Other factors affecting the low tracers' velocities could be the inner curvature of plates at their edges, which made the slope smaller; flow resistance forces from tracers; or the higher packing factor at low heights due to the presence of both dinner plates (D = 270 mm) and dessert plates (D = 160 mm), which made less water to reach those areas.

Finally, the *use of detergent* did not seem to affect significantly flow inside a dishwasher. Comparing Fig. 10C & E, one would not observe any significant difference on the range of velocity values. Less data was obtained for case E due to a lower radioactivity of the tracers used.

3.3.2. Residence times

Residence time plots indicate the average absolute time the tracer spent in every cell location. These plots aid to highlight those 'dead zones' of the system in which the fluid flow is low in comparison to the average of the system. This time will be a function of the tracer velocity but not the number of tracer passes.

Fig. 12 shows a contour plot of residence time for a typical dishwasher set-up, with load and detergent, and for the down-flow stage. Regions with higher residence times were found again on walls and crockery areas. The tracer seemed to stay longer at the lower heights of walls (i.e. $Z < 0.1\ Z_{max}$) and at the edges of the bulk

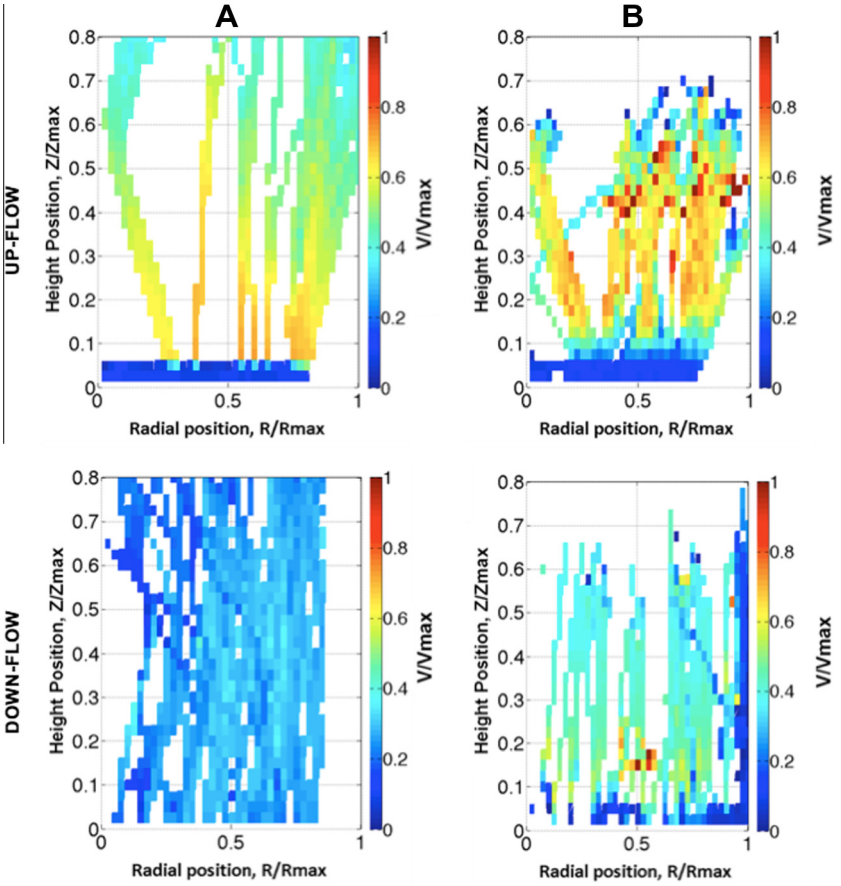

Fig. 13. Eulerian velocity plots for CFD & PEPT data. (A) CFD data. (B) PEPT data. Experimental conditions: Medium pump speed, 'no load' and 'no detergent'.

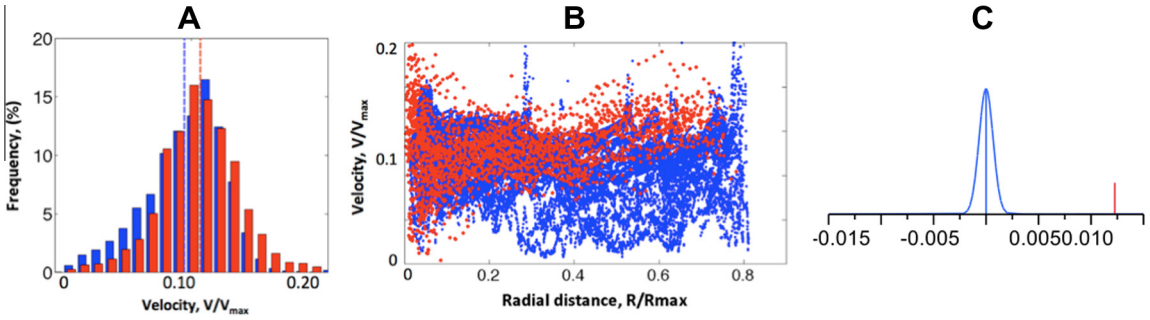

Fig. 14. Comparison between PEPT & CFD data for spray arm locations. (A) velocity histograms. (B) particle paths. (C) statistical *t*-test analysis. Red colour – PEPT data; blue colour – CFD data; red and blue dotted lines in figure A represent average velocity values for PEPT and CFD data respectively. (For interpretation of the references to colour in this figure legend, the reader is referred to the web version of this article.)

of water that remained at the bottom of the dishwasher (i.e. $R \approx R_{max}$). These zones had very low velocity and were stagnant areas. At heights between 0.05 and 0.2 Z_{max}, corresponding to high packing ratio areas, high residence times were observed as well. These regions might potentially enhance chemical processes as the contact between soils and chemicals is produced for longer. They also combined low mechanical input from the appliance.

3.4. CFD and PEPT data comparison

3.4.1. Eulerian comparison

Fig. 13 shows Eulerian velocity contours for (A) CFD and (B) PEPT data. Experimental and simulated conditions were: medium pump speed, 'no load' and 'no detergent'. The same division between up-flow and down-flow was also carried out. In the first row, which contains the spray arm and ejection steps, a similar distribution of water was observed. PEPT data is noisier than CFD, as a consequence of the variability and perturbations occurring in real-life experiments. The gap in water distribution seen in PEPT data at around 0.35 R_{max} of radial distance was also observed for CFD data. Also, CFD plot shows another distribution gap at around 0.5 R_{max}. Slight velocity differences were also observed in the vicinity of spray arm ejections (around 0.05 Z_{max}). While CFD data showed a sudden change in velocity as the water exits the spray arm, the velocity profile estimated using PEPT data was not so abrupt. This phenomenon will be discussed in more detail when analysing individual particle paths (see Section 3.4.2).

In the second row of Fig. 13, velocity contours representing the down-flow stage are shown. In CFD simulations (A) it was not possible to distinguish the flow down the sidewalls. An analogy for

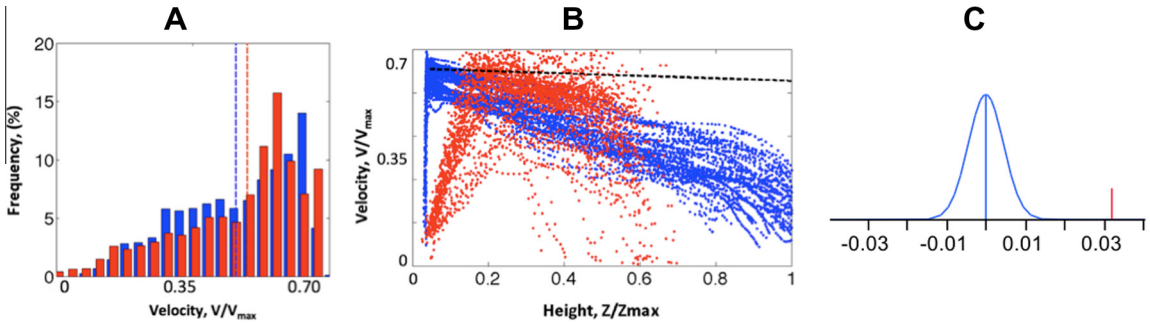

Fig. 15. Comparison between PEPT & CFD data for up-flow locations. (A) Velocity histograms. (B) particle paths. (C) Statistical *t*-test analysis. Red colour – PEPT data; blue colour – CFD data; red and blue dotted lines in figure A represent average velocity values for PEPT and CFD data respectively. Black dotted line in figure B represents gravity deceleration expected. (For interpretation of the references to colour in this figure legend, the reader is referred to the web version of this article.)

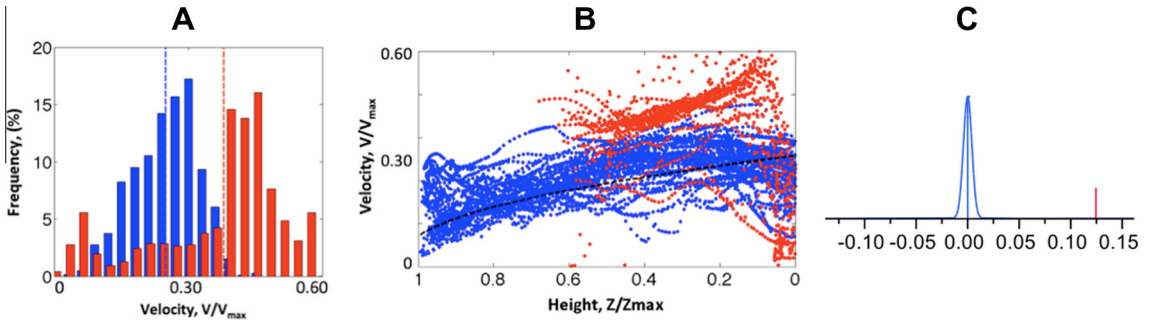

Fig. 16. Comparison between PEPT & CFD data for down-flow locations. (A) Velocity histograms. (B) Particle paths. (C) Statistical *t*-test analysis. Red colour – PEPT data; Blue colour – CFD data; Red and blue dotted lines in figure A represent average velocity values for PEPT and CFD data respectively. Black dotted line in figure B represents gravity deceleration expected. (For interpretation of the references to colour in this figure legend, the reader is referred to the web version of this article.)

this flow would be raindrops falling down a window: wide range of velocities depending on the amount of water falling. At low radial distances, free falling movement was captured by CFD. Although a homogeneous range of velocity was obtained over most of the area, higher velocity values were found for PEPT data.

3.4.2. Particle paths comparison

Fig. 14 shows a velocity comparison for spray arm particle paths locations. Red colour represents PEPT data, while CFD data is shown in blue colour. In column A, all tracer velocities associated to every location were represented in a histogram. The figure shows good initial agreement in terms of velocity distributions. Mean values, represented by both dotted lines, show a slight higher average velocity for PEPT data. In column B, individual particle locations and its associated velocity can be seen. As radial distance increased, PEPT tracer velocity tended to increase as well. CFD data was more uniform, in agreement with a typical Hagen-Poisseuille velocity profile [26]. As a consequence, less overlap between PEPT and CFD data occurred. This slight increase in PEPT tracer velocity suggests that the sudden acceleration effect produced at the nozzle exits might had affected as well the velocity of the tracer as it passes close to those areas. In column C, a statistical *t*-test comparison is shown. The bell-shaped curve represents all variability within CFD values. For data not to have a statistical significant difference, the red line, representing the average PEPT data, should be contained within the curve. This statistical difference is explained by the lack of lower PEPT velocity values at high radial distances. It is in agreement with the data shown in both columns A and B.

In Fig. 15, a similar comparison for particle velocities in the up-flow stage can be seen. In column A, velocity distributions obtained during the ejection step were in good agreement, with a slight higher average velocity for PEPT data. In column B, particle velocities as a function of height position are shown. The highest velocity values for PEPT data were found at higher axial distances than for CFD data. This is a consequence of the fitting routine applied to calculate Lagrangian velocities and commented in Section 2.3.2. Moving intervals of '*n*' data points were always taken to find the 'best fit' line for a central tracer location. Whenever there was an abrupt change in the tracer velocity or in its direction, as it occurred at the nozzle exits of the spray arm, a delay in the velocity change was introduced. The routine always took low velocity locations from the inside of the spray arm to estimate velocities near the outlet of the nozzles, even though '*n*' was small. As a consequence, velocity values were calculated by using low and high velocity tracer locations. Therefore, a lag distance is introduced. The delay in the response from the tracer particle highlighted with the Stokes number is a factor as well of the deviation found in this area. Tracer responded later to an external disturbance when compared to water particles.

The abrupt velocity change seen for CFD data at the water jet exits was due to the application of Bernoulli's Equation (1) in the computer model. As the height difference from the inside of the nozzle to the outside was negligible, the change in velocity given was a function of the pressure difference. Changing the diameter of the nozzles can also change the ejection velocity. The bigger

Table 3
Dimensionless velocity mean and standard deviations values for PEPT and CFD data.

Step/type of data	PEPT		CFD	
	Mean (V_{mean}/V_{max})	STD (V_{mean}/V_{max})	Mean	STD
Spray arm	0.11	0.03	0.10	0.03
Ejection	0.55	0.23	0.52	0.16
Downfall	0.36	0.15	0.24	0.07

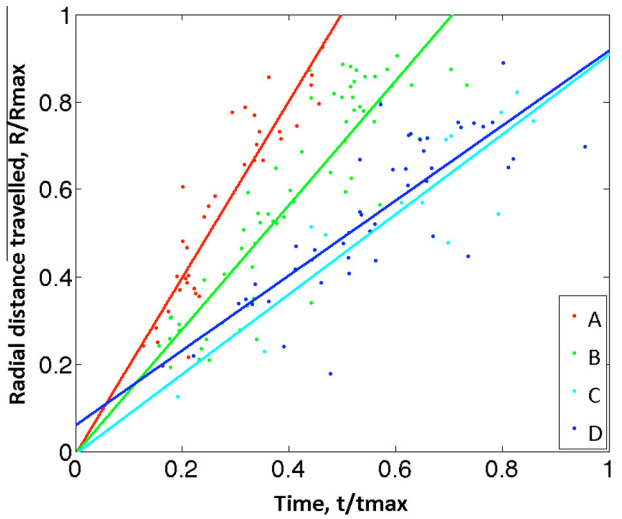

Fig. 17. Radial distance travelled by the tracers vs. time in spray arm until ejection. (A) High pump speed, no detergent; (B) medium pump speed, no detergent; (C) low pump speed, no detergent; (D) low pump speed, detergent.

Table 4
Dimensionless mean velocity comparison inside the spray arm between the two methods. Standard deviation values are shown in brackets. method A – averaged velocity from all Lagrangian data points for each experimental set-up; method B – velocity estimated by dividing the distance travelled by a tracer in the spray arm before ejected and the time taken.

Experiment/ type of data	High pump speed	Medium pump speed	Low pump speed	Low pump speed
	No detergent			With detergent
Method A	0.120 (0.048)	0.084 (0.584)	0.051 (0.025)	0.054 (0.024)
Method B	0.120	0.085	0.055	0.051

the outlet area, the slower the ejection velocity to maintain a constant flow rate:

$$\frac{V^2}{2g}+\frac{P}{\rho g}+z=\text{constant} \quad (1)$$

Outliers from PEPT data can also be seen. These are represented by those locations outside the main cloud of points and are responsible of the variability of PEPT data. They appeared when the tracer travelled at high velocities and PEPT cameras could not collect enough data points or when the radioactivity of the tracer was not high enough. Processing routines were not able to correct entirely the presence of these points. Limitations in the field of view of PEPT cameras were also observed. No locations were collected at height positions above 0.6 Z_{max}.

Gravity deceleration is represented by the black dotted line. It can be seen that for both types of data, the deceleration was higher than the expected by only gravity action. Air resistances for water simulated particles and tracer movement on the ejection may explain the deceleration observed.

In column C, a statistical *t*-test to compare both data sets is shown. The bell-shaped curve represents the variability within CFD data. A significant difference was obtained as the red line, representing the average PEPT velocity value, was found at the right side of the curve. The difference was produced by the lack of PEPT data above 0.6 Z_{max}. Lower velocities expected above this height were not found and this increased PEPT tracer velocity average value.

Finally, in Fig. 16, the comparison was done for the down-flow stage. Only free fall data was used to compare this stage. A significant difference was observed in the histogram shown in column A. Although the distribution shape was similar, there was a clear displacement from CFD data to PEPT data. PEPT data shows higher downfall velocities than those predicted by CFD. In column B, representing particle locations and its associated velocities, PEPT cloud of points was found at higher velocities than CFD cloud. No PEPT data was again observed at heights above 0.6 Z_{max}. At height positions lower than 0.1 Z_{max}, the velocity of PEPT tracer decreased as it reached the bottom part of the dishwasher. A smooth velocity transition was again observed, which relates to the constraints of the processing routine used. As the tracer reached the bulk of the water at the bottom, its velocity should have decreased sharply. Gravity acceleration is shown as the black dotted line. The line indicates that an initial velocity from the roof of the dishwasher is necessary to match PEPT data. This suggests some energy carry-over of the tracer after the impact on the top. No clear reason was found to explain this phenomenon. Inner elasticity of the tracer might have produced a bouncing off effect at the roof of the dishwasher. Also, Stokes number showed a high value for tracer particles. This would explain a different behaviour between simulated water particles and PEPT tracers when impacting the roof. In column C, the statistical *t*-test comparison shows a significant difference between CFD and PEPT data as expected.

In Table 3, absolute mean values and standard deviations were calculated for every distribution shown before. Results matched well for the spray arm and ejection steps and differences were found in the downfall part.

3.5. Alternative analysis: velocity characterisation in the spray arm

In Fig. 17, the time the tracers spent inside the spray arm is shown as a function of the radial position from which they were ejected. Data from four different experimental set-ups was represented: (A) high pump speed, no detergent; (B) medium pump speed, no detergent; (C) low pump speed, no detergent; (D) low pump speed, detergent. Each data point shown represents a single pass of the tracer through the spray arm. A linear trend was obtained for each of the experimental conditions. By calculating the slopes, the average velocity of the tracer inside the spray arm was calculated. Table 4 shows a comparison between the averaged velocity estimated using all Lagrangian data available for each case (method A) and the velocity values calculated through this alternative method (method B).

The different pump speeds had a noticeable effect. As pump head increased, the slopes of the trend lines, and therefore, their average velocity values increased as well. The effect of detergent on flow is proved again negligible. Both lines obtained at same pump speed (A & D) did not show variance in the slope given and they overlapped well.

4. Conclusions

Water motion inside a household ADW has been described via PEPT. Data processing has introduced newly developed algorithm to enhance data quality by including smoothing and interpolation routines.

Analysis of the data has shown how a typical water sequence can be divided into the following stages: movement inside pumps and spray arms, ejection, impact, downfall (over walls, crockery or free falling) and residence in the bulk water remaining at the bottom.

Jets paths have been determined to follow a straight line for a fixed position and time, so their study can be discretised and ana-

lysed as a vector problem. A specific dishwasher location is impacted at a frequency rate related to the rotational speed of the spray arms.

The Eulerian velocity analysis has shown that the highest velocities over the whole sequence are found on the ejection stage. Energy provided by the pump is the main factor affecting velocities in the spray arm and ejection stages, although its influence was shown to be negligible during the downfall process. At this latter stage, the main difference in flow was found in those areas with high packing density of crockery, where there was little space for the tracer to move. The low velocity profiles seen suggest a low shear distribution over most of the crockery loaded as tracers were washed down very slowly. The homogeneous low velocity profile found in crockery areas also suggested a small coverage from the high velocity water films (before film jump) generated after the impact of jets over different crockery surfaces.

Residence time analysis has highlighted lower wall areas and edges of the bottom bulk of water as those areas where tracers stayed for longer times, and therefore, that can be considered as stagnant zones. Some high residence values have been also found in crockery areas with high packing density. This could benefit chemistry availability and interaction with soils in those zones.

A comparison between PEPT and CFD data has been also done for a case with an empty dishwasher (no load or basket in the inner volume). Good agreement has been achieved for spray arm and ejection steps. However, differences have appeared in the downfall free falling profile. A hypothesis is that the PEPT tracer bounces off at the roof of the dishwasher creating a higher velocity profile than predicted by CFD.

Finally, alternative analyses have shown a negligible effect of detergent in water flow.

Results and conclusions made through this work are being used to develop a mathematical model that describes the effect of different design parameters (dishwasher dimensions, spray arm design or crockery distribution) on the spray of water in different dishwasher areas, impact frequencies on different items and direct impingement coverage.

Acknowledgements

This research was founded by the Engineering and Physical Sciences Research Council (EPSRC) and industrially sponsored by Procter & Gamble (P&G). The authors would like to thank Zayeed Alam from Procter & Gamble, Blair D. Mikkelsen, Praveen Poojary and Ketan Parashar from Whirlpool Corporation for their help on Computational Fluid Dynamics and hardware and also to Prof. David Parker, Dr. Thomas Leadbeater and Dr. Joseph Gargiulli for their assistance and guidance during the realisation of the experimental work.

References

[1] P. Berkholz, R. Stamminger, G. Wnuk, J. Owens, S. Bernarde, Manual dishwashing habits: an empirical analysis of UK consumers, Int. J. Consum. Stud. 34 (2010) 235–242, http://dx.doi.org/10.1111/j.1470-6431.2009.00840.x.

[2] E.C. for E. Standardization, Electric dishwashers for household use – Methods for measuring the performance, 2012.

[3] M. De Paepe, E. Theuns, S. Lenaers, J. Van Loon, Heat recovery system for dishwashers, Appl. Therm. Eng. 23 (2003) 743–756, http://dx.doi.org/10.1016/s1359-4311(03)00016-4.

[4] M. Weiss, M. Patel, M. Junginger, K. Blok, Analyzing price and efficiency dynamics of large appliances with the experience curve approach, Energy Policy 38 (2010) 770–783, http://dx.doi.org/10.1016/j.enpol.2009.10.022.

[5] C. Asteasu, J. Astiazaran, J. Besga, A dishwasher design system: an application of tailor-made CAD systems versus commercial systems, Comput. Graph. 16 (1993) 395–399, http://dx.doi.org/10.1016/0097-8493(92)90026-R.

[6] P.J. Fryer, K. Asteriadou, A prototype cleaning map: a classification of industrial cleaning processes, Trends Food Sci. Technol. 20 (2009) (2009) 255–262, http://dx.doi.org/10.1016/j.tifs.2009.03.005.

[7] T. Wang, J.F. Davidson, D.I. Wilson, Effect of surfactant on flow patterns and draining films created by a static horizontal liquid jet impinging on a vertical surface at low flow rates, Chem. Eng. Sci. 88 (2013) 79–94, http://dx.doi.org/10.1016/j.ces.2012.11.009.

[8] X. Liu, J.H. Lienhard, The hydraulic jump in circular jet impingement and in other thin liquid films, Exp. Fluids 116 (1993) 108–116, http://dx.doi.org/10.1007/BF00190950.

[9] D.I. Wilson, B.L. Le, H.D.a. Dao, K.Y. Lai, K.R. Morison, J.F. Davidson, Surface flow and drainage films created by horizontal impinging liquid jets, Chem. Eng. Sci. 68 (2012) 449–460, http://dx.doi.org/10.1016/j.ces.2011.10.003.

[10] T. Wang, D. Faria, L.J. Stevens, J.S.C. Tan, J.F. Davidson, D.I. Wilson, Flow patterns and draining films created by horizontal and inclined coherent water jets impinging on vertical walls, Chem. Eng. Sci. 102 (2013) 585–601, http://dx.doi.org/10.1016/j.ces.2013.08.054.

[11] D.J. Parker, C.J. Broadbent, P. Fowles, M.R. Hawkesworth, P. McNeil, Positron emission particle tracking – a technique for studying flow within engineering equipment, Nucl. Instrum. Methods Phys. Res. Sect. A 326 (1993) 592–607, http://dx.doi.org/10.1016/0168-9002(93)90864-E.

[12] M. Barigou, Particle tracking in opaque mixing systems: an overview of the capabilities of PEP and PEPT, Chem. Eng. Res. Des. 82 (2004) 1258–1267, http://dx.doi.org/10.1205/cerd.82.9.1258.44160.

[13] S. Bakalis, P.J. Fryer, D.J. Parker, Measuring velocity distributions of viscous fluids using positron emission particle tracking (PEPT), AIChE J. 50 (2004) 1606–1613, http://dx.doi.org/10.1002/aic.10153.

[14] M. Rafiee, M.J.H. Simmons, A. Ingram, E.H. Stitt, Development of positron emission particle tracking for studying laminar mixing in Kenics static mixer, Chem. Eng. Res. Des. 91 (2013) 2106–2113, http://dx.doi.org/10.1016/j.cherd.2013.05.022.

[15] D.J. Parker, a.E. Dijkstra, T.W. Martin, J.P.K. Seville, Positron emission particle tracking studies of spherical particle motion in rotating drums, Chem. Eng. Sci. 52 (1997) 2011–2022, http://dx.doi.org/10.1016/S0009-2509(97)00030-4.

[16] L.S. Bbosa, I. Govender, A.N. Mainza, M.S. Powell, Power draw estimations in experimental tumbling mills using PEPT, Miner. Eng. 24 (2011) 319–324, http://dx.doi.org/10.1016/j.mineng.2010.10.005.

[17] Y.L. Ding, R. Forster, J.P.K. Seville, D.J. Parker, Segregation of granular flow in the transverse plane of a rolling mode rotating drum, Int. J. Multiph. Flow 28 (2002) 635–663, http://dx.doi.org/10.1016/S0301-9322(01)00081-7.

[18] C. Mac Namara, a. Gabriele, C. Amador, S. Bakalis, Dynamics of textile motion in a front-loading domestic washing machine, Chem. Eng. Sci. 75 (2012) 14–27, http://dx.doi.org/10.1016/j.ces.2012.03.009.

[19] M. Eesa, M. Barigou, Horizontal laminar flow of coarse nearly-neutrally buoyant particles in non-Newtonian conveying fluids: CFD and PEPT experiments compared, Int. J. Multiph. Flow 34 (2008) 997–1007, http://dx.doi.org/10.1016/j.ijmultiphaseflow.2008.06.003.

[20] L. Liu, M. Barigou, Numerical modelling of velocity field and phase distribution in dense monodisperse solid–liquid suspensions under different regimes of agitation: CFD and PEPT experiments, Chem. Eng. Sci. 101 (2013) 837–850, http://dx.doi.org/10.1016/j.ces.2013.05.066.

[21] P. Pianko-Oprych, a.W. Nienow, M. Barigou, Positron emission particle tracking (PEPT) compared to particle image velocimetry (PIV) for studying the flow generated by a pitched-blade turbine in single phase and multi-phase systems, Chem. Eng. Sci. 64 (2009) 4955–4968, http://dx.doi.org/10.1016/j.ces.2009.08.003.

[22] AHAM, AHAM DW-1: Household Electric Dishwashers by Association of Home Appliance Manufacturers, United States of America, 1992.

[23] D.J. Parker, X. Fan, Positron emission particle tracking—application and labelling techniques, Particuology 6 (2008) 16–23, http://dx.doi.org/10.1016/j.cpart.2007.10.004.

[24] J.A. Schetz, A.E. Fuhs (Eds.), Handbook of Fluid Dynamics and Fluid Machinery: Fundamentals of Fluid Dynamics, John Wiley & Sons Inc, 1996, http://dx.doi.org/10.1002/9780470172636.

[25] F. Chiti, S. Bakalis, W. Bujalski, M. Barigou, A. Eaglesham, A.W. Nienow, Using positron emission particle tracking (PEPT) to study the turbulent flow in a baffled vessel agitated by a Rushton turbine: improving data treatment and validation, Chem. Eng. Res. Des. 89 (2011) 1947–1960, http://dx.doi.org/10.1016/j.cherd.2011.01.015.

[26] R.B. Bird, W.E. Stewart, E.N. Lightfoot, Transport Phenomena, John Wiley & Sons, 2007.